Chinese Chemical Letters 36 (2025) 110131

Contents lists available at ScienceDirect

Chinese Chemical Letters

journal homepage: www.elsevier.com/locate/cclet

A novel PEC-EC dual-mode biosensing platform for dual target detection of miRNA-133a and cTnI

Hejie Zheng, Zhili Wang, Guizhen Luo, Cuicui Du, Xiaohua Zhang*, Jinhua Chen*

State Key Laboratory of Chemo/Biosensing and Chemometrics, College of Chemistry and Chemical Engineering, Hunan University, Changsha 410082, China

ARTICLE INFO

Article history:
Received 29 February 2024
Revised 6 June 2024
Accepted 14 June 2024
Available online 15 June 2024

Keywords:
Photoelectrochemical assay
Electrochemical assay
Dual-mode
Dual-target
miRNA-133a
cTnI

ABSTRACT

MicroRNA-133a (miRNA-133a) and cardiac troponin I (cTnI) are different-type crucial biomarkers of acute myocardial infarction (AMI), whose levels are great significance for AMI diagnosis and treatment. Herein, a novel photoelectrochemical-electrochemical (PEC-EC) dual-mode biosensing platform for dual-target assays of miRNA-133a and cTnI was developed. In which, a PEC-EC dual-mode sensing platform for miRNA-133a was constructed based on the changes of the photocurrent inhibition effect and the electrochemical signal of Fc on the Fc-hairpin DNA probe (Fc-HP)/ZnCdS-quantum dots (QDs)/ITO electrode. Furthermore, under magnetic separation and the specific interaction between cTnI and its aptamer, the N-doped porous carbon-ZnO polyhedra (NPC-ZnO)-hemin-capture DNA probe hybrid (NH-CP) was obtained and introduced to the Fc-HP/ZnCdS-QDs/ITO electrode *via* hybridization between NH-CP and Fc-HP. The hemin molecules encapsulated in NH-CP could effectively induce the photocurrent-polarity-switching of the Fc-HP/ZnCdS-QDs/ITO electrode and generate a new electrochemical signal originating from hemin. Thus, cTnI was assayed sensitively and selectively by the PEC-EC dual-mode biosensing platform. Here, Fc and hemin not only serve as the electrochemical indicators, but also respectively inhibit the photocurrent and switch the photocurrent polarity of ZnCdS-QDs. Furthermore, the proposed biosensing platform could be easily expanded to the detection of other multiplex-type biomarkers *via* the change of the sequences of the related DNA probes, implying its significant potential in clinical diagnosis and biological analysis.

Acute myocardial infarction (AMI) is a prevalent cardiovascular disease that can cause irreversible damage to the heart and even threaten human life [1]. Therefore, early accurate diagnosis is greatly crucial for the prevention and treatment of AMI. To date, a variety of AMI-related biomarkers have been found, such as microRNAs (miRNA-133a, miRNA-499, miRNA-21, miRNA-199a and miRNA-1) [2-4], cardiac troponins (cTnI, cTnC and cTnT) [5], myoglobin [6] and creatine kinase [7]. In which, the single-stranded miRNA-133a plays a significant role in mediating cardiac processes [2]. Meanwhile, cTnI has higher specificity and sensitivity compared with the other two cardiac troponins, which is considered as the "gold standard" for diagnosing AMI [8]. The expression peaks of miRNA-133a and cTnI in plasma almost simultaneously appear after the occurrence of AMI [9]. Nevertheless, miRNA-133a is associated with several cancers, including lung cancer [10], gastric cancer [11], bladder cancer and hepatocellular carcinoma [12]. And abnormal cTnI level also might be caused by other cardiac diseases including acute pericarditis, heart failure, acute inflammatory myocarditis and end-stage renal disease. [8,13]. Consequently, the assay on a single biomarker may lead to false positive results in clinical diagnosis of AMI.

Compared with single-biomarker detection, multiple-biomarker assay can improve the accuracy and detection efficiency in biological analysis and clinical diagnosis [14,15]. For example, Sun *et al.* constructed an electrochemiluminescence (ECL) sensing platform based on AuNPs@G-quadruplex spherical nucleic acid enzyme for detecting miRNA-133a and miRNA-499 [16]. Gupta *et al.* designed a label-free electrochemical (EC) multi-analyte immunosensing platform for the simultaneous detection of three cardiac markers using a nine-electrodes array fixed with different capture probes [17]. Nonetheless, the current studies have only achieved the individual detection of nucleic acids or proteins for AMI assay. The analysis of different-type biomarker can manifest more comprehensive information and avoid false positive diagnoses [18]. Therefore, it is necessary to construct a biosensing platform for the detection of different-type AMI biomarkers [19,20].

At present, great progress has been made in the single-mode analysis methods for AMI biomarkers, such as ECL [9], photoelectrochemical (PEC) [21], EC [22], fluorescence (FL) [23] and enzyme-

* Corresponding authors.
E-mail addresses: mickyxie@hnu.edu.cn (X. Zhang), chenjinhua@hnu.edu.cn (J. Chen).

https://doi.org/10.1016/j.cclet.2024.110131
1001-8417/

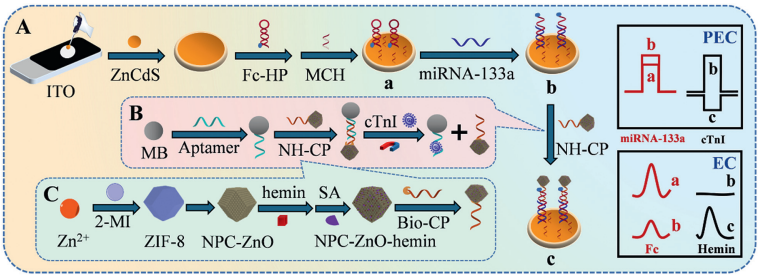

Scheme 1. (A) Schematic diagram of the PEC-EC dual-mode biosensing platform for detection of miRNA-133a and cTnI. (B) The process of the cTnI recognition and magnetic separation. (C) The preparation procedure of NH-CP.

linked immunosorbent assays [24]. However, the quantitative assay *via* single-mode output may still be affected by manipulation, experimental and instrumental errors, as well as background signals [25]. The construction of dual-mode biosensing platform with different response mechanisms can not only resolve above issues, but also provide mutual cross-validation of the detection results in different modes [26]. Recently, several dual-mode sensing platforms have been proposed, including ECL-FL [27], PEC-EC [25], photoelectrochemical-colorimetric (PEC-CL) [28] and FL-CL [29]. Among which, the emerging PEC technique cooperated with EC has attracted increasing concerns as a new generation of analysis methods, due to their rapid response, easy operation, high sensitivity and simple instruments [22,30,31]. For example, our group successfully constructed an EC-PEC biosensing platform, achieving the sensitive and selective assay of miRNA-210 [25].

On the other hand, the EC biosensors usually quantify analytes by collecting electrochemical response signals from the redox tag as an indicator, such as ferrocene (Fc), methylene blue and hemin, based on the target-induced "signal-off" or "signal-on" strategy [32,33]. Similarly, the traditional PEC sensing strategies are primarily divided into "signal-off" [26] and "signal-on" [34] methods according to the relationship between PEC response and target concentration. Recently, an interesting PEC sensing strategy, named as the photocurrent-polarity-switching method [35], was developed to effectively minimizing the occurrence of the false-positive or false-negative signals caused by the interferents, and thus improve the selectivity and accuracy. For these PEC sensing strategies, an effective signal probe is generally essential to inhibit, amplify or switch PEC signal [26,34,35]. Based on the above consideration, the multifunctional signal indicators/probes are of great significance for developing a simple and efficient PEC-EC biosensing platform.

Herein, a novel dual-target biosensing platform based on PEC-EC dual modes was constructed for detecting different-type AMI biomarker of miRNA-133a and cTnI, based on the inhibition effect of Fc and the photocurrent-polarity-switching ability of hemin towards the PEC responses of ZnCdS quantum dots (ZnCdS-QDs, ZCS), as well as the electrochemical properties of Fc and hemin. ZCS were used as the basic photoelectric materials due to their outstanding photoelectric properties, adjustable band gap, easy modification and good stability [36,37]. As shown in Scheme 1, the Fc-labeling hairpin DNA (Fc-HP) was immobilized on the ZCS/indium tin oxide (ITO) electrode *via* the Cd–S bond. Upon the introduction of miRNA-133a, the hairpin structure of Fc-HP was opened and Fc was far away from the electrode surface, leading to an enhanced photocurrent and a decreased Fc electrochemical oxidation peak current. Afterward, a dual-mode PEC-EC sensing platform was further constructed for cTnI detection. In which, the N-doped porous carbon-ZnO (NPC-ZnO) ployhedra-hemin-capture DNA probe (NH-CP) conjugates were firstly prepared by encapsulating hemin into NPC-ZnO, whose surface was modified with streptavidin (SA) and further combined with biotin-labeling capture probe (Bio-CP). Then, the NH-CP would hybridize with the aptamer of cTnI modified on the magnetic beads (MB-Apt) to form the NH-CP/MB-Apt conjugates. When cTnI is present, NH-CP was released due to the specific recognition of aptamer toward cTnI, and further hybridized with the Fc-HP opened by miRNA-133a. Then, the hemin encapsulated in NH-CP would induce the photocurrent polarity switching of ZCS, and meanwhile generate a new electrochemical signal. Thus, cTnI could also be sensitively and selectively detected. Here, Fc and hemin not only serve as the electrochemical indicators, but also respectively inhibit the photocurrent and switch the photocurrent polarity of ZCS. Furthermore, the proposed biosensing platform could be easily expanded to the detection of other multiplex-type biomarkers *via* the change of the sequences of the related DNA probes, implying its significant potential in clinical diagnosis and biological analysis.

The morphologies of ZIF-8, NPC-ZnO and NPC-ZnO-hemin are revealed by scanning electron microscopy (SEM) images in Fig. 1. As can be clearly observed, ZIF-8 (Fig. 1A) is a typical rhombic dodecahedron with an average particle size of ~120 nm. After calcination of ZIF-8, the derived NPC-ZnO (Fig. 1B) composite materials inherit the original dodecahedron structure with a slightly smaller particle size (~110 nm) than that of ZIF-8 polyhedra. When hemin is incorporated in NPC-ZnO, the morphology and the size of NPC-ZnO-hemin (Fig. 1C) keep the same as that of the pristine NPC-ZnO. On the other hand, the X-ray diffraction (XRD) analysis was carried out to investigate the structures of ZIF-8 and NPC-ZnO. As displayed in Fig. 1D, the strong characteristic diffraction peaks of ZIF-8 (curve a) illustrate its high crystallinity, well matching with the reported work [38]. After calcination, the typical peaks of ZIF-8 disappear, indicating that the crystal structure of ZIF-8 is completely destroyed and NPC-ZnO is successfully prepared as reported in literature [38].

To demonstrate the successful encapsulation of hemin into the pores of NPC-ZnO, nitrogen adsorption-desorption isotherms were collected for NPC-ZnO-hemin and NPC-ZnO as displayed in Fig. 1E. The Brunauer-Emmett-Teller (BET) specific surface area and pore volume of NPC-ZnO polyhedrane measured to be 484.7 m^2/g and 0.578 cm^3/g, respectively. By contrast, the sharp decrease in the specific surface area (92.6 m^2/g) and pore volume (0.191 cm^3/g) of NPC-ZnO-hemin confirms the successful embedding of hemin in NPC-ZnO. The porous structure with large specific surface area of NPC-ZnO polyhedra is favorable for the encapsulation of hemin, which facilitates the EC and photocurrent-polarity-switching PEC responses induced by sufficient hemin. In addition, the optical properties of NPC-ZnO, hemin and NPC-ZnO-hemin were characterized by UV–vis absorption spectroscopy as shown in Fig. 1F. Compared with NPC-ZnO (curve a), NPC-ZnO-hemin (curve c) shows a strong absorption peak at ~395 nm similar to hemin (curve b) [39], which is ascribed to the incorporation of hemin into NPC-ZnO polyhedra. In addition, the morphology, structure and elemental chemical states of ZCS were characterized and the results show that ZCS with an average diameter of ~6 nm have been successfully prepared (Figs. S1 and S2 in Supporting information). The carboxy-

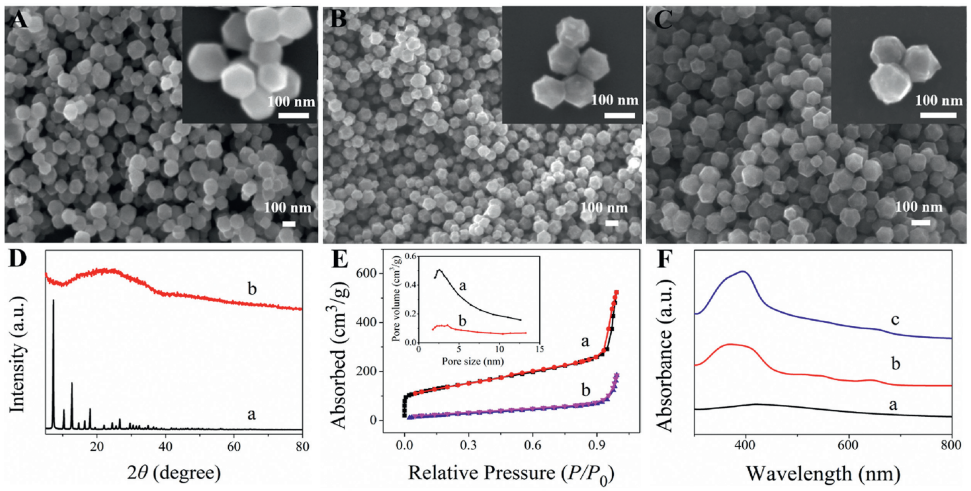

Fig. 1. SEM images and the corresponding high-magnification images (insets) of (A) ZIF-8, (B) NPC-ZnO and (C) NPC-ZnO-hemin. (D) XRD patterns of (a) ZIF-8 and (b) NPC-ZnO. (E) Nitrogen adsorption-desorption isotherms of (a) NPC-ZnO and (b) NPC-ZnO-hemin. (F) UV–vis spectra of (a) NPC-ZnO, (b) hemin and (c) NPC-ZnO-hemin.

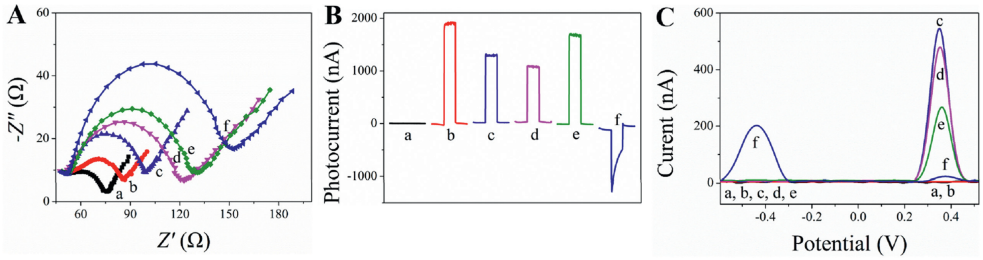

Fig. 2. (A) Nyquist plots of different electrodes in the solution containing 5 mol/L $[Fe(CN)_6]^{3-/4-}$ and 0.1 mol/L KCl (frequency ranging from 100 kHz to 0.1 Hz; amplitude, 5 mV). (B) Photocurrent responses of different electrodes in 0.1 mol/L Tris–HCl (pH 7.4) containing 0.1 mol/L AA at 0 V. (C) Square wave voltammetry (SWV) responses of different electrodes in 0.1 mol/L Tris–HCl (pH 7.4). (a) ITO, (b) ZCS/ITO, (c) Fc-HP/ZCS/ITO, (d) MCH/Fc-HP/ZCS/ITO, (e) miRNA-133a/MCH/Fc-HP/ZCS/ITO, (f) NH-CP/miRNA-133a/MCH/Fc-HP/ZCS/ITO.

lated MB were characterized by SEM, XRD and Fourier transform infrared (FT-IR) spectroscopy and its successful preparation is confirmed (Fig. S3 in Supporting information).

The stepwise assembly process of the developed dual-mode dual-target biosensing platform was investigated by electrochemical impedance spectroscopy (EIS). As is well-known, the semicircle diameters of the Nyquist plots reflect the interfacial charge transfer resistance (R_{ct}) of the electrodes. It can be clearly observed in Fig. 2A, the R_{ct} value of ZCS/ITO (curve b, 35 Ω) is larger than that of the ITO electrode (curve a, 25 Ω) due to the semiconductor property of ZCS. The successive assembly of Fc-HP (curves c, 49 Ω) and MCH (curves d, 72 Ω) on the surface of ZCS/ITO results in a continuous increase of the R_{ct} values, due to the hindrance of DNA molecules and the blocking effect of MCH. When the electrode is further incubated with miRNA-133a (curve e, 80 Ω) and NH-CP (curve f, 102 Ω) released by cTnI, the R_{ct} values of the related electrodes become larger gradually, owing to steric hindrance effects of NH-CP. Above EIS results confirm that the successful building of the AMI-biomarkers biosensing platform according to Scheme 1.

The PEC and EC responses of the different modification electrodes were also investigated during the step-by-step construction process. As shown in Figs. 2B and C, there is no obvious photocurrent or electrochemical response from the bare ITO electrode (curve a). However, the ZCS/ITO electrode (curve b) exhibits an obvious anodic PEC signal due to the excellent photoelectric properties of ZCS, yet no obvious EC signal. After Fc-HP is immobilized on the ZCS/ITO electrode (curve c), the photocurrent is weakened significantly owing to the inhibition effect of Fc toward ZCS/ITO electrode, and a remarkable electrochemical oxidation peak emerges at ~0.38 V ascribed to the proximity of the Fc electrochemical indicator to the ZCS/ITO electrode. Then, the PEC and EC responses of the electrode would be slightly weakened after sealing the non-specific sites with MCH (curve d), mainly resulted from the blocking effect of MCH. In the presence of miRNA-133a (curve e), the hairpin structure of Fc-HP is opened and Fc is far away from the electrode surface, which results in an increase in the photocurrent of the electrode and a decrease in the Fc electrochemical oxidation peak current.

After further incubated with NH-CP conjugates released by cTnI (curve f), the photocurrent polarity is switched, leading to a significant cathodic photocurrent. The outstanding ability of hemin to switch the photocurrent polarity of the ZCS/ITO electrode was further demonstrated as shown in Fig. S4 (Supporting information), which is beneficial to the high sensitivity and selectivity of the PEC biosensing platform with negative background signal. Meanwhile, a new electrochemical oxidation current peak of hemin can be observed at –0.41 V. In addition, the PEC mechanisms for the inhibiting effect of Fc and hemin-induced photocurrent-polarity-switching of the ZCS/ITO electrode were described in Scheme S1 (Supporting information) based on the energy band positions obtained from Fig. S5 (Supporting information) and the literatures [35,40]. The above results convincingly reveal that the PEC-EC biosensing platform was successfully constructed and can be used for sensitive miRNA-133a and cTnI assays.

Under the optimal experimental conditions (Fig. S6 in Supporting information), the analytical performance of the proposed dual-mode dual-target biosensing platform for AMI biomarker assay was investigated. For PEC biosensing of miRNA-133a (Fig. 3A), the anodic photocurrent increases as increasing the

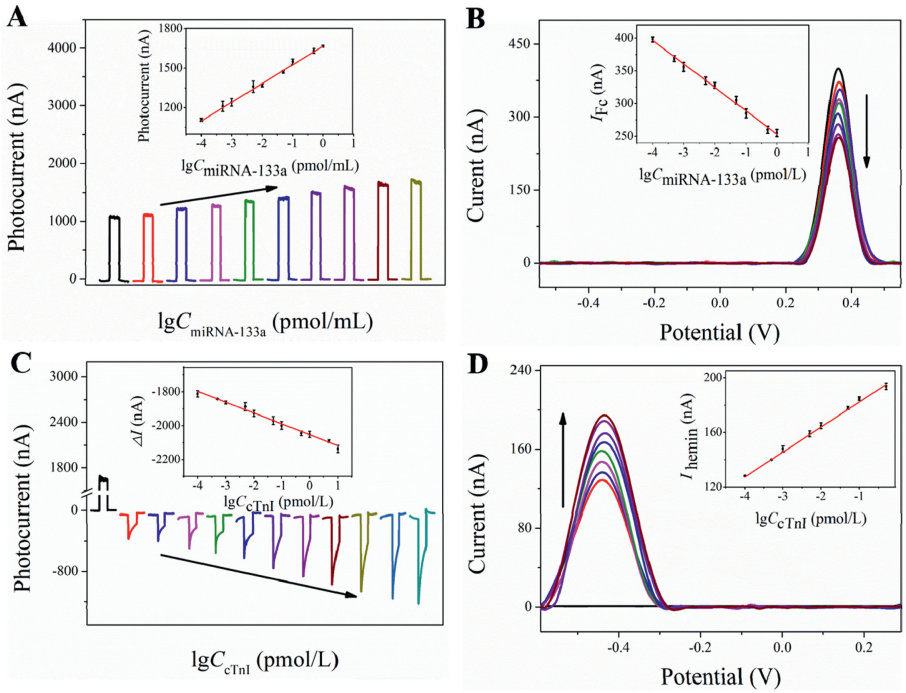

Fig. 3. (A) Photocurrents responses and (B) SWV responses to different concentration of $C_{miRNA\text{-}133a}$: 0, 0.0001, 0.0005, 0.001, 0.005, 0.01, 0.05, 0.1, 0.5 and 1 pmol/L. Inset: (A) Photocurrents and (B) I_{Fc} *versus* $lgC_{miRNA\text{-}133a}$ calibration plot. (C) Photocurrents responses to different concentration of C_{cTnI}: 0, 0.0001, 0.0005, 0.001, 0.005, 0.01, 0.05, 0.1, 0.5, 1, 5 and 10 pmol/L. (D) SWV responses to different concentration of C_{cTnI}: 0, 0.0001, 0.0005, 0.001, 0.005, 0.01, 0.05, 0.1, and 0.5 pmol/L. Inset: (C) Photocurrents and (D) I_{hemin} *versus* lgC_{cTnI} calibration plot.

concentration of miRNA-133a, which is proportional to the logarithm of the miRNA-133a concentration ($lgC_{miRNA\text{-}133a}$) ranging from 0.1 fmol/L to 1 pmol/L. A regression equation of I (nA) = 141.80$lgC_{miRNA\text{-}133a}$ + 1667.43 (R^2 = 0.9977) is obtained with a detection limit of 0.032 fmol/L (S/N = 3). For the EC assay of miRNA-133a, the electrochemical signals of Fc decrease with the increase of the miRNA-133a concentration. The linear relationship between the oxidation peak current of Fc (I_{Fc}) and the logarithm of miRNA-133a concentration is observed from 0.1 fmol/L to 1 pmol/L (Fig. 3B). The linear equation is I_{Fc} (nA) = −35.88$lgC_{miRNA\text{-}133a}$ + 253.14 (R^2 = 0.9957) and the corresponding detection limit is calculated to be 0.054 fmol/L (S/N = 3). Furthermore, a PEC-EC biosensing platform was constructed for the detection of cTnI under sufficient miRNA-133a ($C_{miRNA\text{-}133a}$ = 1 pmol/L). As shown by the PEC assay in Fig. 3C, a large anodic photocurrent is observed without cTnI, which is switched to an obvious cathodic photocurrent when the NH-CP conjugates released by cTnI is introduced to the sensing system. High sensitivity can be achieved based on the negative background signal originated from the polarity switching of photocurrent [41,42]. The cathodic photocurrent responses increase with the increase of the cTnI concentration. A linear relationship between the value of the change in photocurrent (ΔI) and the logarithm of the cTnI concentration is acquired in the range from 0.1 fmol/L to 10 pmol/L (3 fg/mL to 30 pg/mL), with a linear equation of ΔI (nA) = −64.12lgC_{cTnI} − 2052.89 (R^2 = 0.9971) and a detection limit of 0.034 fmol/L (1.02 fg/mL, S/N = 3). For EC biosensing of cTnI (Fig. 3D), the oxidation peak current of hemin increases as the concentration of cTnI increases. Consequently, the linear regression equation is I_{hemin} = 18.40lgC_{cTnI} + 200.86 (R^2 = 0.9968) with a linear response range of 0.1 fmol/L to 500 fmol/L (3 fg/mL to 15 pg/mL) and a detection limit of 0.041 fmol/L (1.23 fg/mL, S/N = 3). Therefore, the different-type AMI biomarkers of miRNA-133a and cTnI can be sensitively assayed by the developed PEC-EC dual-target biosensing platform which shows better analytical performance compared with most other reported methods (Table S2 in Supporting information).

In assessing the practicality of the developed biosensing platform, further investigation was conducted to examine its selectivity. For miRNA-133a assay, miRNA-21, miRNA-141, miRNA-155, miRNA-210 and miRNA-101 were used as the interferents. As shown in Fig. S7A (Supporting information), no obvious changes of PEC or EC signals are found in response to the five interferents, whereas significant responses for both sensing modes are observed toward the miRNA-133a target. Besides, the (photo)current values of the biosensing platform for the mixture of miRNA-133a and interferents are almost the same as these for only miRNA-133a. The obtained results reveal the satisfactory selectivity of the developed PEC-EC biosensing platform for miRNA-133a assay. On the other hand, human serum albumin (HSA), prostate specific antigen (PSA), immunoglobulin G (IgG), carcinoembryonic antigen (CEA) and vascular endothelial growth factor 165 (VEGF165) were selected as the interferents for assessing the selectivity in the dual-mode biosensing of cTnI [43,44]. From Fig. S7B (Supporting information), it is noted that the five interferents weaken the anodic photocurrent compared with the blank sample but cannot switch the polarity of the photocurrent. Only the presence of cTnI could induce the switching of the photocurrent polarity and generate an obvious cathodic photocurrent. Meanwhile, the cathodic photocurrent for the mixture of cTnI and interferents is almost the same as that for the cTnI sample. In terms of the EC sensing of cTnI, much larger electrochemical signals are observed for cTnI and the mixture compared to these five interferents. These results demonstrate that the constructed PEC-EC dual-mode biosensing platform also has excellent selectivity for cTnI assay.

The stability and reproducibility of the constructed PEC-EC biosensing platform were also studied. The PEC responses under 10 times “on-off” irradiation cycles indicate an acceptable PEC stability (Fig. S8A in Supporting information). In addition, the stability also was investigated by storing the designed biosensing platform

at 4 °C for 15 days as presented in Fig. S8B (Supporting information). The PEC and EC signals for miRNA-133a (1 pmol/L) assay still remain about 96.5% (curve a) and 92.1% (curve b) of the initial values. For cTnI (500 fmol/L) biosensing, the PEC and EC responses are 93.1% (curve c) and 94.3% (curve d) of the initial values. Additionally, the reproducibility of the developed biosensing platform was also assessed on six independent electrodes. As shown in Fig. S9A (Supporting information), the relative standard deviation (RSD) values of the PEC and EC responses for miRNA-133a assay are 5.5% and 4.8%, respectively. For cTnI biosensing platform (Fig. S9B in Supporting information), the RSD values are 5.3% and 5.1% respectively for the PEC and EC modes. These results suggest the satisfactory stability and reproducibility of the proposed PEC-EC biosensing platform for the dual-target assay.

In order to validate the applicability of the proposed PEC-EC biosensing platform in complex samples, different concentrations of miRNA-133a and cTnI were spiked in 20-fold diluted human serum samples, and the recovery experiments were performed. As displayed in Table S3 (Supporting information), the recoveries of the developed dual-mode sensing platform for the dual targets of miRNA-133a and cTnI are acceptable. The abovementioned results indicate the great potential of the developed PEC-EC dual-target biosensing platform in the practical assays of miRNA-133a and cTnI in complex samples.

In summary, a novel PEC-EC dual-mode dual-target biosensing platform is developed for sensitive and selective assays of miRNA-133a and cTnI which are the different-type AMI biomarkers. Based on the inhibition effect of Fc toward the photocurrent of ZCS and the electrochemical activity of Fc, miRNA-133a can be detected by the photoelectrochemical (electrochemical) method with a linear range of 0.1 fmol/L to 1 pmol/L and a detection limit of 0.032 fmol/L (0.054 fmol/L). Furthermore, cTnI can be detected by PEC-EC dual-mode sensing strategy based on the photocurrent polarity-switching abilities of hemin toward ZCS and the electrochemical activity of hemin. The linear ranges from 0.1 fmol/L to 10 pmol/L (PEC) and 0.1 fmol/L to 500 fmol/L (EC), as well as a detection limits of 0.034 fmol/L (PEC) and 0.041 fmol/L (EC), are achieved. For the proposed PEC-EC dual-mode biosensing platform, Fc and hemin not only serve as the electrochemical indicators, but also respectively inhibits the photocurrent and switches the photocurrent polarity of ZCS. In addition, this dual-mode biosensing platform exhibits good selectivity, stability, reproducibility, and potential applicability for detecting miRNA-133a and cTnI in complex biological systems. Furthermore, the proposed biosensing platform could be easily expanded to the detection of other multiplex-type biomarkers *via* the change of the sequences of the related DNA probes, implying its significant potential in clinical diagnosis and biological analysis.

Ethical agreement

The blood samples from healthy adult donors were provided from Hunan University Hospital (Changsha, China) and informed consent was obtained from the volunteers. All sample preparations were approved by the Institutional Review Committee of relevant hospital and carried out in accordance with institutional guidelines and conformed to the relevant regulatory ethical standards.

Declaration of competing interest

The authors declare that they have no known competing financial interests or personal relationships that could have appeared to influence the work reported in this paper.

CRediT authorship contribution statement

Hejie Zheng: Writing – original draft, Investigation, Data curation, Conceptualization. **Zhili Wang:** Validation, Data curation. **Guizhen Luo:** Validation, Data curation. **Cuicui Du:** Writing – review & editing, Validation, Data curation. **Xiaohua Zhang:** Writing – review & editing, Validation, Data curation. **Jinhua Chen:** Writing – review & editing, Supervision, Project administration, Methodology, Conceptualization.

Acknowledgment

This work was financially supported by National Natural Science Foundation of China (Nos. 22074033, 22374035).

Supplementary materials

Supplementary material associated with this article can be found, in the online version, at doi:10.1016/j.cclet.2024.110131.

References

[1] A. Pourali, M.R. Rashidi, J. Barar, G. Pavon-Djavid, Y. Omidi, Trends Anal. Chem. 134 (2021) 116123.
[2] X. Cheng, D.D. Ren, G.H. Xu, et al., Biosens. Bioelectron. 196 (2022) 113706.
[3] Y.D. Sun, L. Shi, Q.W. Wang, L. Mi, T. Li, Anal. Chem. 91 (2019) 3652–3658.
[4] W.Q. Zhang, J. Ling, D. Wen, et al., Sens. Actuators B 371 (2022) 132484.
[5] D.P. Sun, X.G. Lin, J. Lu, et al., Biosens. Bioelectron. 142 (2019) 111578.
[6] X.L. Yang, Y. Zhao, L.J. Sun, et al., Sens. Actuators B 257 (2018) 60–67.
[7] X.N. Mi, H. Li, R. Tan, Y.F. Tu, Anal. Chem. 92 (2020) 14640–14647.
[8] L.C. Duque-Ossa, B. Garcia-Ferrera, J.A. Reyes-Retana, Curr. Probl. Cardiol. 48 (2023) 101067.
[9] L.Y. Yu, L.P. Zhu, M.X. Yan, et al., Anal. Chem. 93 (2021) 11809–11815.
[10] M. Xu, Y.Z. Wang, Oncol. Rep. 30 (2013) 1398–1404.
[11] J. Yu, X.F. Cao, Y. Zheng, L.Q. Yan, J.W. Wang, Mol. Med. Rep. 18 (2018) 5023–5029.
[12] X. Chen, L.H. Bo, X. Zhao, Q. Chen, Mol. Med. Rep. 11 (2015) 3900–3907.
[13] Z.P. Yuan, L. Wang, J. Chen, et al., Analyst 146 (2021) 5474–5495.
[14] Q.Q. Cai, H.K. Li, B. Wang, G.F. Jie, Chem. Eng. J. 476 (2023) 146799.
[15] J.F. Chang, W.X. Lv, J.H. Wu, H.Y. Li, F. Li, Chin. Chem. Lett. 32 (2021) 775–778.
[16] Y.D. Sun, Q.W. Wang, L. Mi, L. Shi, T. Li, Anal. Chem. 91 (2019) 12948–12953.
[17] R.K. Gupta, R. Pandya, T. Sieffert, M. Meyyappan, J.E. Koehne, J. Electroanal. Chem. 773 (2016) 53–62.
[18] Y.M. Nie, P. Zhang, H.J. Wang, et al., Anal. Chem. 89 (2017) 12821–12827.
[19] S.Y. Chen, Z.C. Yu, Y.S. Wan, et al., Anal. Chem. 95 (2023) 14494–14501.
[20] Z.C. Yu, H.X. Gong, J.H. Xu, et al., Anal. Chem. 94 (2022) 7408–7416.
[21] M.J. Hao, P. Miao, Y. Wang, et al., Anal. Chem. 93 (2021) 11251–11258.
[22] X.N. Mi, H. Li, R. Tan, B.N. Feng, Y.F. Tu, Biosens. Bioelectron. 192 (2021) 113482.
[23] X.J. Wu, H. Yang, W. Li, et al., Sens. Actuators B 344 (2021) 130315.
[24] Y.Q. Wang, T. Liu, M. Yang, et al., Biosens. Bioelectron. 193 (2021) 113554.
[25] Q.Q. Zhang, S.Y. Liu, C.C. Du, et al., Anal. Chem. 93 (2021) 14272–14279.
[26] R.Y. Yang, G.H. Jiang, H.M. Liu, et al., Biosens. Bioelectron. 188 (2021) 113337.
[27] X.S. Gao, H.K. Li, Y. Zhao, G.F. Jie, Biosens. Bioelectron. 143 (2019) 111602.
[28] Y.Y. Cheng, R.M. Kong, W.A. Hu, et al., Chin. Chem. Lett. 34 (2023) 107502.
[29] J.J. Deng, W.J. Ma, P. Yu, L.Q. Mao, Anal. Chem. 87 (2015) 6958–6965.
[30] Y.T. Zhou, S.Z. Lv, X.Y. Wang, L.Y. Kong, S. Bi, Anal. Chem. 94 (2022) 14492–14501.
[31] H.J. Wang, L. Guo, Q.Y. Du, et al., Anal. Chem. 96 (2024) 581–589.
[32] E.H. Xiong, Z.Z. Li, X.H. Zhang, et al., Anal. Chem. 89 (2017) 8830–8835.
[33] Y.Q. Liu, E.H. Xiong, X.Y. Li, et al., Biosens. Bioelectron. 87 (2017) 970–975.
[34] X.Y. Zhang, L. Han, L.D. Yu, et al., ACS Appl. Mater. Interfaces 13 (2021) 15881–15889.
[35] Y.M. Fu, Q. Yu, Q.Q. Zhang, et al., Biosens. Bioelectron. 192 (2021) 113547.
[36] T.T. Wu, Y.R. Zhang, D. Wei, et al., Sens. Actuators B 256 (2018) 812–819.
[37] M. Chen, X. Huang, C. Chen, W.Q. Hou, Y.M. Xu, Appl. Catal. B 298 (2021) 120469.
[38] R.Y. Yang, X.X. Yan, Y.M. Li, X.H. Zhang, J.H. Chen, ACS Appl. Mater. Interfaces 9 (2017) 42482–42491.
[39] R.Y. Yang, J. Liu, J. Electroanal. Chem. 873 (2020) 114346.
[40] L.X. Meng, Y.M. Li, R.Y. Yang, et al., Chem. Commun. 55 (2019) 2182–2185.
[41] L.L. Lu, R.J. Zeng, Q.Y. Lin, X. Huang, D.P. Tang, Anal. Chem. 95 (2023) 16335–16342.
[42] R.J. Zeng, J.H. Xu, T.K. Liang, M.J. Li, D.P. Tang, ACS Sens. 8 (2023) 317–325.
[43] L.T. Huang, G.N. Cai, R.J. Zeng, Z.C. Yu, D.P. Tang, Anal. Chem. 94 (2022) 9487–9495.
[44] Y. Gao, M.J. Li, Y.Y. Zeng, X.L. Liu, D.P. Tang, Anal. Chem. 94 (2022) 13582–13589.